buildings

MDPI

Article

Analysis of Circumferential and Longitudinal Non-Uniformity of Steel Corrosion in Concrete Subjected to Mechanical Load

Bingliu Wu [1,2], Ke Xu [3], Mingchang Yang [3], Zheng Dong [3,4], Jianwen Shao [1,2,*], Chuanqing Fu [3,4] and Wenhao Ni [5]

1 The Architectural Design & Research Institute of Zhejiang University Co., Ltd., Hangzhou 310058, China; tmgcwbl2005@163.com
2 Center for Balance Architecture, Zhejiang University, Hangzhou 310058, China
3 College of Civil Engineering, Zhejiang University of Technology, Hangzhou 310023, China; 201806080523@zjut.edu.cn (K.X.); 221123060125@zjut.edu.cn (M.Y.); zdong@zjut.edu.cn (Z.D.); chqfu@zjut.edu.cn (C.F.)
4 Zhejiang Key Laboratory of Civil Engineering Structures & Disaster Prevention and Mitigation Technology, Hangzhou 310023, China
5 Hangzhou Landscape Architecture Design Institute Co., Ltd., Hangzhou 310030, China; niwenhaohotmail@163.com
* Correspondence: concrzjut@126.com

Abstract: Reinforcement corrosion significantly impacts the service life of reinforced concrete structures. The present study investigates the circumferential and longitudinal non-uniformity of steel corrosion in concrete subjected to mechanical load. Results indicate that, in the case of steel corrosion in concrete subjected to mechanical load, the distribution of rust layer thickness around the perimeter of the steel bar is fitted well with a Gaussian distribution. As the corrosion rate gradually increases, the uniform coefficient is linearly proportional to the minimum thickness of the rust layer. With respect to the longitudinal non-uniformity of steel corrosion, load-induced transverse cracks have a significant impact on the non-uniformity of corrosion, leading to the formation of rust peaks near the locations of transverse cracks. In the vicinity of each rust peak, the corrosion rate of the steel bar follows a Gaussian distribution. With respect to the non-uniformity of corrosion along the longitudinal rebar, a Gumbel distribution is identified to fit well, both in the cases of the non-stressed section and the pure bending section, although with dissimilar non-uniform parameters. Crack coefficients (α and β) are introduced to describe the influence of transverse cracks on the longitudinal non-uniformity of steel corrosion.

Keywords: steel corrosion; non-uniform corrosion; load-induced transverse cracks; Gaussian distribution; Gumbel distribution

check for updates

Citation: Wu, B.; Xu, K.; Yang, M.; Dong, Z.; Shao, J.; Fu, C.; Ni, W. Analysis of Circumferential and Longitudinal Non-Uniformity of Steel Corrosion in Concrete Subjected to Mechanical Load. *Buildings* **2024**, *14*, 509. https://doi.org/10.3390/buildings14020509

Academic Editors: Alberto Taliercio and Grzegorz Ludwik Golewski

Received: 5 January 2024
Revised: 25 January 2024
Accepted: 9 February 2024
Published: 13 February 2024

Copyright: © 2024 by the authors. Licensee MDPI, Basel, Switzerland. This article is an open access article distributed under the terms and conditions of the Creative Commons Attribution (CC BY) license (https://creativecommons.org/licenses/by/4.0/).

1. Introduction

Steel corrosion is one of the main causes which degrade the durability of reinforced concrete (RC) structures [1,2]. The volume of corrosion products generated by steel corrosion is 2–6 times the volume of original non-corroded steel [3]. The accumulation of corrosion products in concrete produces expansion force, resulting in the cracking of the concrete protective layer. Corrosion reduces the bearing capacity and increases the possibility of failure for RC structures exposed to marine environments [4–8]. In this regard, the evaluation of steel corrosion is of great significance in predicting the service life of RC structures. The corrosion of steel in RC structures is caused by carbonation or ingress of aggressive agents like chlorides. Carbonation leads to a decrease in pH in the concrete pore solution, where the corrosion could be generally uniform. Chloride ions, on the other hand, induce local breakdown of the passive film on the surface of steel. In this regard, the chloride-induced corrosion of steel in RC structures propagates non-uniformly [1,3,9]. There are mainly two types of indexes to characterize the non-uniform corrosion of steel bars, including

parameters for circumferential non-uniformity and longitudinal non-uniformity. The pitting factor and the cross-sectional area spatial heterogeneity factor have been investigated to quantify the longitudinal non-uniformity of steel corrosion. The former parameter (i.e., pitting factor) mainly describes the pitting depth of corroded steel. The latter (i.e., the cross-sectional area spatial heterogeneity factor) is used to quantify the variation in the cross-sectional area along the length of steel [10,11]. Based on the longitudinal non-uniformity parameters, the load-bearing capacity of corroded RC beams or columns is predicted [6,7]. In terms of the circumferential non-uniformity (i.e., the non-uniformity around the perimeter of the steel bar), a Gaussian function has been identified to fit well with the corrosion pattern [3]. The circumferential non-uniformity of corroded steel is associated with the corrosion-induced cracking of concrete [11]. Nevertheless, in addition to severe environments, RC structures are inevitably subjected to mechanical load, which leads to the cracking of concrete. The load-induced cracks potentially accelerate the ingress of aggressive agents like chlorides into concrete and alter the restraint of concrete on the corrosion of steel, thereby affecting the corrosion pattern [12]. In this regard, it is necessary to investigate the non-uniformity of the corrosion of steel in concrete subjected to mechanical load. However, few studies consider the influence of load-induced cracks on the non-uniformity of steel corrosion.

With respect to the investigation of reinforcement corrosion, the accelerated corrosion method has been widely used as it shortens the period of experiments. Several electrical accelerated corrosion test methods are employed, including the soaking method [10], part soaking method [13,14], and embedded auxiliary electrode method [15,16]. Notedly, these accelerated corrosion methods induce uniform corrosion, while the corrosion of steel bars in concrete subjected to natural conditions is non-uniform in most cases [3,17]. In this regard, it is of great importance to employ a non-uniform accelerated corrosion method, mimicking the corrosion pattern of steel in concrete under natural conditions.

The research object of the present study is the corrosion of steel in RC beams under mechanical loading conditions. A non-uniform accelerated corrosion method was utilized to simulate the non-uniform corrosion of reinforcing steel in natural environments. The circumferential non-uniformity and the longitudinal non-uniformity of steel corrosion in concrete subjected to mechanical load were investigated and analyzed.

2. Materials and Methods

2.1. Materials and Specimen Fabrication

The dimensions of the RC beam are 100 mm × 180 mm × 1800 mm. The longitudinal steel bar of the beam is an HRB 335 steel bar with a diameter of 12 mm. HRB 235 steel bars with a diameter of 6 mm are employed as the stirrups [18]. The size of the longitudinal steel bar is similar to the U.S. size of #4 while the stirrup is similar to the U.S. size of #2. Notedly, the steel bars used in the present study were manufactured in China, and their size is not exactly the same as the U.S. size. The thickness of concrete is 15 mm, as shown in Figure 1.

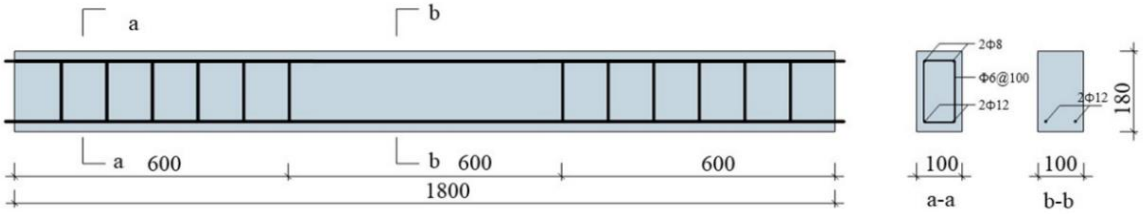


Figure 1. Dimensions of RC beam (mm). Letters a and b represent two cross-section shown in the figure.

Table 1 lists the concrete mix proportion. The concrete specimen was cured for 28 days in a standard curing room with a temperature of 20 °C and a relative humidity of 90% after casting. The compressive strength of the concrete after 28 days was 49.6 MPa.

Table 1. Concrete mix proportion.

Water Binder Ratio	Cement (kg/m^3)	Water (kg/m^3)	Coarse Aggregate (kg/m^3)	Fine Aggregate (kg/m^3)
0.53	375	200	1125	750

Figure 2 demonstrates the loading system which consists of four springs, four corresponding screws, and six backing plates. The spring was compressed by twisting the screw cap on the upper part of the screw, thereby applying load to the RC beam. During the loading process, a crack-measuring instrument with an accuracy of 0.01 mm was used to measure the transverse cracks on the surface of the test beam. The loading was stopped when the maximum transverse crack width reached 0.2 mm, and the remaining nuts were tightened after the loading was stopped.

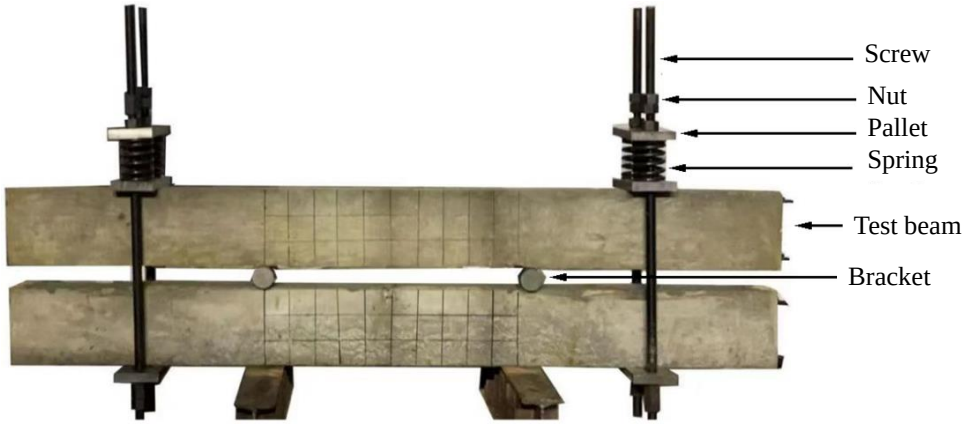


Figure 2. Loading system.

2.2. Accelerated Non-Uniform Corrosion

The corrosion of steel bars in concrete in natural environments is non-uniform corrosion, where the corrosion is more serious on the side of steel near the surface of the concrete. In this regard, an accelerated corrosion method developed by the authors is utilized to induce non-uniform corrosion of steel [2]. As shown in Figure 3, stainless steel is embedded in concrete, working as an auxiliary electrode. In this method, the steel bar is regarded as the anode, and the stainless steel wire as the cathode. The diameter of the stainless steel wire is far less than the steel bar, i.e., 0.5 mm. The spacing between the stainless steel wire and the steel bar is 5 mm. As depicted in Figure 3, L_n represents the distance between the stainless steel wire and the surface of the steel bar. During the accelerated corrosion process, the distance between the stainless steel wire and the surface of the steel bar varies at different positions along the steel surface. The greater the distance between a specific point on the surface of the corroded steel bar and the stainless steel wire, the higher the resistance of the corresponding pore solution. This is because the voltage between the two electrodes is fixed. Consequently, as the distance between the surface of the steel bar and the stainless steel wire increases, the current density decreases, resulting in non-uniform rust formation. Hence, the corrosion degree is higher on the side of the steel bar closer to the stainless steel wire, while the corrosion degree on the surface of the steel bar away from the stainless steel wire is relatively lower. Based on the authors' previous studies, the accelerated non-uniform corrosion method shown in Figure 3 induces a distribution of rust thickness that can be well-fit by the Gaussian model, which is similar to that of natural corrosion [2,16].

The RC beam was soaked in a 5% sodium chloride solution for 72 h before the accelerated corrosion, to moisturize the concrete beam. During accelerated corrosion, the specimen was wrapped with a wet sponge. In order to prevent the loss of water during the experiment, a layer of plastic wrap is wrapped around the sponge and the sodium chloride

solution is sprayed regularly around the specimen. DC voltage is applied between the stainless steel wire and the steel bar during an accelerated corrosion test, where the steel bar is connected to the positive electrode of the power supply, and the stainless steel wire is connected to the negative electrode of the power supply.

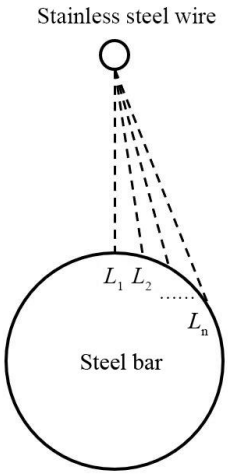


Figure 3. Schematic diagram of the principle of non-uniform corrosion.

The period for the duration of accelerated corrosion was set to be 16 d, 48 d, 96 d, and 132 d, respectively. A small value of impressed current density (i.e., 20 μA/cm^2) was used. Under such a small value of impressed current density, the expansion coefficient of corrosion products can be similar to that of natural corrosion [19]. The value of impressed current density was kept constant during the accelerated corrosion test. Different values of corrosion degrees were achieved in the cases of various corrosion periods. According to Faraday's law, the mass loss of steel bars after the accelerated corrosion test can range from 1% to 8%. It is equivalent to the corrosion degree of steel in RC structures subjected to a natural environment for up to several years [20,21]. Nevertheless, it should be noted that, due to non-uniformity and the galvanic effect, the corrosion degree of steel bars in concrete varies [20].

2.3. Preparation of Samples for the Investigation of Circumferential Non-Uniformity

As the test beam was loaded symmetrically in this test, the right half of the main rebars was taken out to investigate the circumferential non-uniformity of corrosion, while the left half was employed to investigate the longitudinal non-uniformity. To observe the distribution of the rust thickness of the steel reinforcement, concrete slices were cut as shown in Figure 4. These slices were cut from the surface of the concrete specimen after the accelerated corrosion was finished and the surface was cleaned. To prevent damage to the specimen during the cutting process, epoxy resin with low viscosity was added to the crack prior to the cutting process, and the surface of the concrete specimen was coated with epoxy resin. The thickness of each slice was controlled at 3 cm to prevent the concrete sections from being too thin and damaged. The cut samples were sealed in anhydrous ethanol to prevent further oxidation of the steel bars in the air. Before observation, the slices were removed from the anhydrous ethanol and wiped dry. After that, the surface of the sample was polished and cleaned.

The KH-7700 digital microscope produced by HIROX Co., Ltd (Shanghai, China). was employed to observe the rust layer of steel bars. Before the measurement, the steel ruler with the smallest scale of 1 mm was measured using the microscope. The reading of 1 mm was 1004 μm, which was within the allowable error range.

To quantify the area of the rust layer, the cross-sectional area of the corroded steel bar was divided into 36 sections, as demonstrated in Figure 5. The rust layer can be distinguished by color. As can be seen in Figure 5, the silver object is the cross-section of

the steel bar, while the black and brown part around the circumference of the steel bar is the rust layer. The area of corrosion products in each section is measured using the digital microscope at a magnification of 160 times, which is denoted as S_n (n = 1 to 36). The average value for the thickness of the rust layer in each section (T_n) is calculated through Equation (1). The corrosion degree of corroded steel in each concrete slice was calculated through the ratio of the remaining area of the corroded steel bar to the original cross-sectional area of the steel bar.

$$T_n = \frac{S_n}{C_n}, \quad (1)$$

where C_n is the perimeter of the steel bar in each section, and n equals 1 to 36.

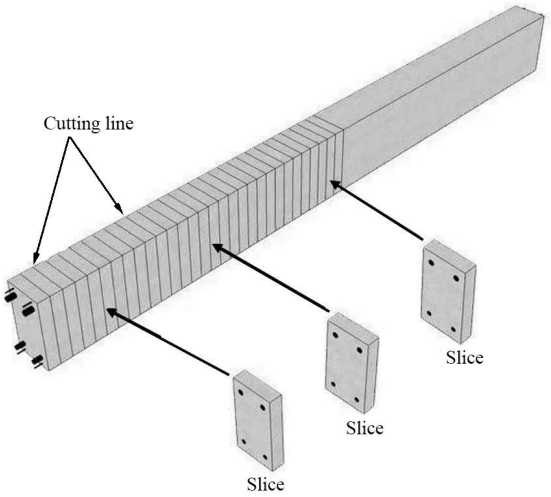


Figure 4. Schematic illustration of cutting process.

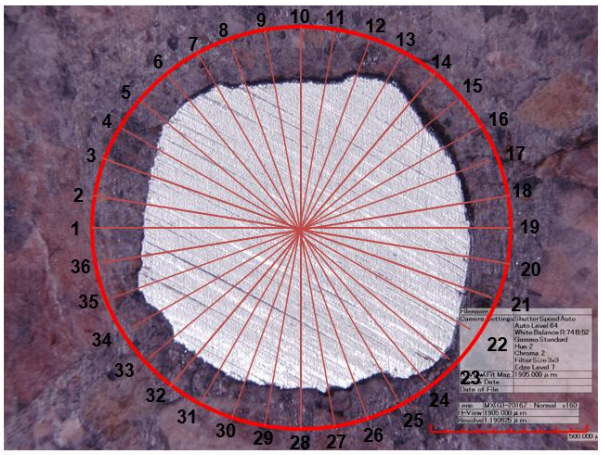


Figure 5. Photograph of the cross-sectional area of corroded steel under the microscope.

2.4. Preparation of Samples for the Investigation of Longitudinal Non-Uniformity

The left half of the main rebars was taken out to investigate the longitudinal non-uniformity of corrosion. For each loading system, there are eight rebars in the tension zone, i.e., the bottom of RC beams. The length of the steel bars is 900 mm. To investigate the influence of stress conditions on the non-uniformity of steel corrosion, the longitudinal steel bars were cut every 300 mm. As such, the longitudinal steel bar in the tension zone was divided into a non-stressed section (0~300 mm), a bending shear section (300~600 mm), and a pure bending section (600~900 mm). The steel bars were cleaned through a mechanical cleaning process which employed a bristle brush, according to ASTM G1-03 [22]. Notedly,

the same cleaning process was performed on non-corroded steel, and the mass loss from the cleaning was found to be negligible.

A Roland-LPX-600DS laser scanner (Roland DG Co., Ltd., Shanghai, China) was used to perform three-dimensional laser scanning of the corroded steel bars, obtaining the morphology of corroding steel. The scanning speed was 37 mm/s with a positioning accuracy of 0.02 mm [19]. Additionally, the scanning process was carried out on a non-corroded steel bar. The average cross-sectional area of the non-corroded steel was taken as the initial cross-sectional area of the steel bar (A_0). The corrosion degree based on loss of cross-sectional area (η) was calculated through Equation (2).

$$\eta = 1 - A_s / A_0, \tag{2}$$

where A_s is the cross-sectional area of the corroded steel bar.

3. Results and Discussion

3.1. Circumferential Non-Uniformity of Steel Corrosion in Concrete Subjected to Mechanical Load

Three models were used to fit the data of the thickness for the rust layer, including the Gaussian model, ellipse model, and linear model. Figure 6 presents the fitting results of the rust layer in the cases of different corrosion degrees. The results of the determination coefficient R^2 are demonstrated in Figure 7. The average values of R^2 for the Gaussian, the ellipse, and the linear models in all cases are 0.894, 0.532, and 0.698, respectively. The Gaussian model displays the best performance in fitting the distribution of thickness for the rust layer. Noticeably, based on the results of the present study, the Gaussian model works well both in the cases of concrete with and without load-induced cracks. The Gaussian distribution used to describe the thickness of the rust layer is expressed as Equation (3) [3].

$$T_r = c + \frac{a}{\sqrt{2\pi}b} \exp\left[-\left(\frac{\theta - \theta_0}{\sqrt{2}b}\right)^2\right] \quad \theta \in \left[-\frac{\pi}{2}, \frac{\pi}{2}\right], \tag{3}$$

where T_r is the thickness of the rust layer, a is the non-uniform coefficient, b is the spread coefficient, and c is the uniform coefficient.

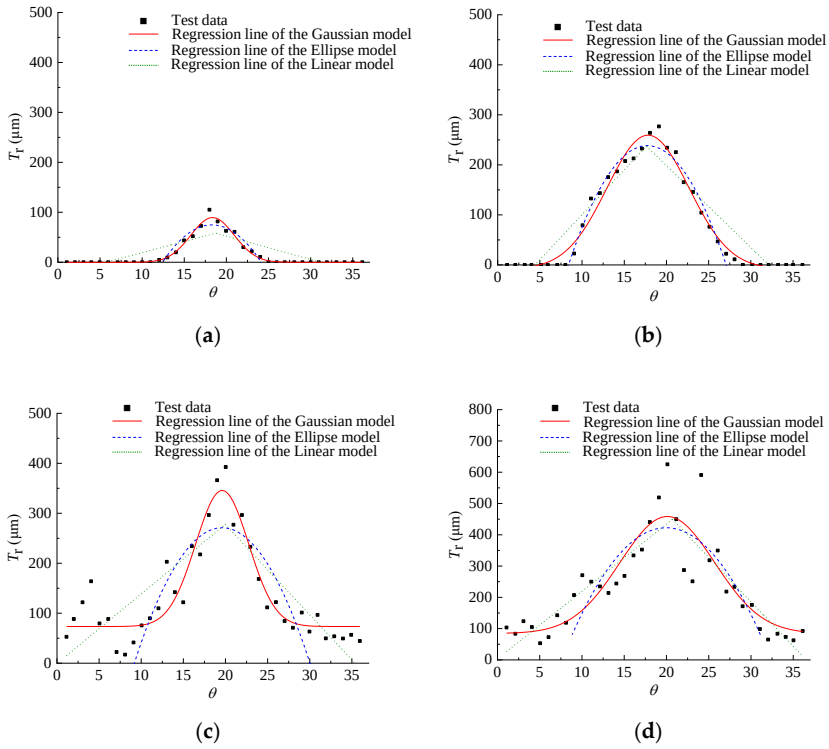


Figure 6. Distribution of rust layers at corrosion degrees of (**a**) 0.4%, (**b**) 1.4%, (**c**) 3.4% and (**d**) 4.7%.

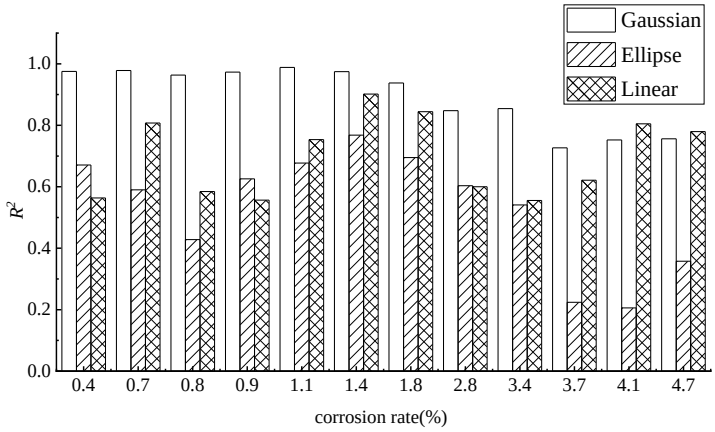


Figure 7. The determination coefficients R^2 of three models in the cases of different corrosion degrees.

Parameter a reflects the degree of non-uniform corrosion of the rebar. With the increase in a, the maximum value of local corrosion of the rebar gradually increases. As illustrated in Figure 8, the peak value of thickness ($T_{\text{r-max}}$) of the rust layer increases with the increasing value of a.

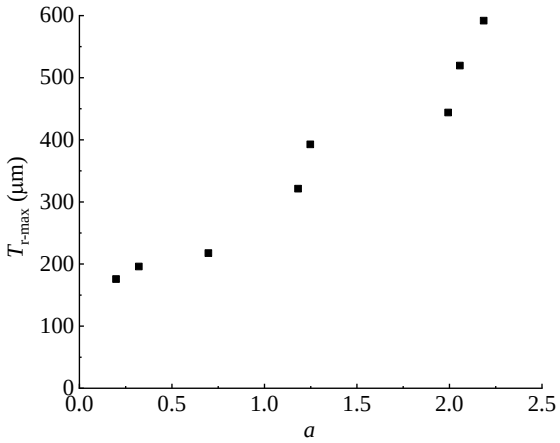


Figure 8. Relationship between non-uniform coefficient (a) and maximum thickness of rust layer ($T_{\text{r-max}}$).

On the other hand, the uniform coefficient c describes the corrosion layer covering the entire circumference of the steel bar. Figure 9 presents the relationship between uniform coefficient c and the minimum value of thickness for the rust layer ($T_{\text{r-min}}$). As the corrosion rate gradually increases, c is linearly proportional to the minimum thickness of the rust layer.

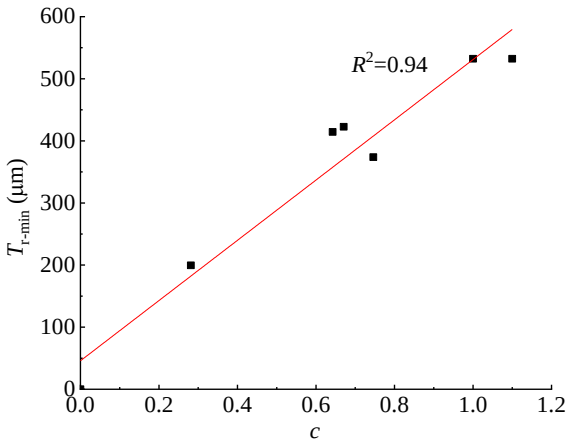


Figure 9. Relationship between uniform coefficient (c) and minimum thickness of rust layer ($T_{\text{r-min}}$).

3.2. Effects of Load-Induced Transverse Cracks on the Longitudinal Non-Uniformity of Steel Corrosion

Based on the 3D scanning, the corrosion rate (η) along the length of the longitudinal steel bar was calculated through Equation (2). The sustained load induces transverse cracks mainly at the bottom of the pure bending section of the RC beams. Figure 10 demonstrates the corrosion rate of steel at different positions of the pure bending section. The red dashed lines in Figure 10 represent the positions of transverse cracks. It can be seen that the corrosion rate distribution of the pure bending section is significantly affected by the transverse cracks. The peaks of corrosion rate appear at, or in the vicinity of, the position of transverse cracks. This is due to the fact that the transverse cracks lower the resistance of the concrete pore solution, thereby increasing the corrosion rate in the cracked region compared to other areas. A similar phenomenon occurs in natural corrosion, where load-induced cracks become the main channel for aggressive agents to enter the surface of longitudinal reinforcement. In this regard, the longitudinal reinforcement at the cracked region is depassivated preferentially. Macrocells are formed between active steel in the cracked region and passive steel in the uncracked region, which further accelerates the corrosion of steel in the cracked region due to the galvanic effect [23,24]. As a result, peaks in the corrosion rate form at the position of transverse cracks.

A Gaussian distribution has been identified to fit well with the non-uniform corrosion along the length of steel reinforcement [25]. With respect to the non-uniform corrosion of the longitudinal rebar in the pure bending section, the Gaussian model (Equation (4)) was used to describe the distribution of longitudinal non-uniform corrosion. Figure 11 shows the fitting results of a typical distribution of corrosion rate in the vicinity of the load-induced transverse crack. As shown in Equation (4), when x equals z, the maximum cross-sectional corrosion rate is obtained. In this regard, the minimum cross-sectional area of the longitudinal bar appears at the position where x is equal to z. Table 2 lists the fitting results of the corroded longitudinal rebar in the pure bending section. A good agreement is demonstrated between the test data and the fitting results in cases of various crack widths.

$$\eta(x) = \frac{a_1}{b_1\sqrt{2\pi}} \exp[-\left(\frac{x-z}{\sqrt{2}b_1}\right)^2] + c_1, \quad (4)$$

where $\eta(x)$ is the corrosion rate at the position of x, z is the position where the maximum corrosion rate occurs, a_1 and b_1 are coefficients related to the longitudinal non-uniformity, and c_1 is the coefficient related to the uniform part of corrosion.

Figure 12 depicts the results of coefficients a_1, b_1, and c_1 in the cases of different crack widths. Coefficients a_1 and b_1, which are related to the non-uniformity of corrosion for the longitudinal rebar, increase with increasing crack width. The uniform coefficient c_1 is generally constant in the cases of dissimilar crack widths. It can be calculated that the limit of corrosion rate ($\eta(x)$) shown in Equation (4) in the case of an extremely large value of x equals the value of the uniform coefficient of longitudinal non-uniformity (c_1). As expressed in Equation (5), when the value of x approaches infinity, the result of $\eta(x)$ approximates c_1. This indicates that, when the region of steel is far away from the position of the load-induced transverse crack, the value of the corrosion rate approaches a constant value, which is c_1. In this regard, the value of the uniform coefficient herein is independent of the transverse cracks and is more correlated to the corrosion degree of the whole longitudinal rebar. For each longitudinal rebar at the bottom of the RC beam, the corrosion rate of the whole steel bar was calculated and the average value of c_1 was obtained, as shown in Figure 13. The difference between the corrosion rate of the whole steel bar and the value of c_1 is regarded as the non-uniform proportion of longitudinal steel bar corrosion. As the corrosion rate increases, the proportion of uniform parts increases, while the proportion of non-uniform parts decreases. This indicates that the corrosion of steel bars tends to be

more uniform with an increasing corrosion rate, and the longitudinal non-uniformity of steel bars is significant when the corrosion rate is low.

$$\lim_{x\to\infty}\eta(x)=\lim_{x\to\infty}\left[\frac{a_1}{b_1\sqrt{2\pi}}e^{-\left(\frac{x-z}{\sqrt{2}b_1}\right)^2}+c_1\right]=c_1, \tag{5}$$

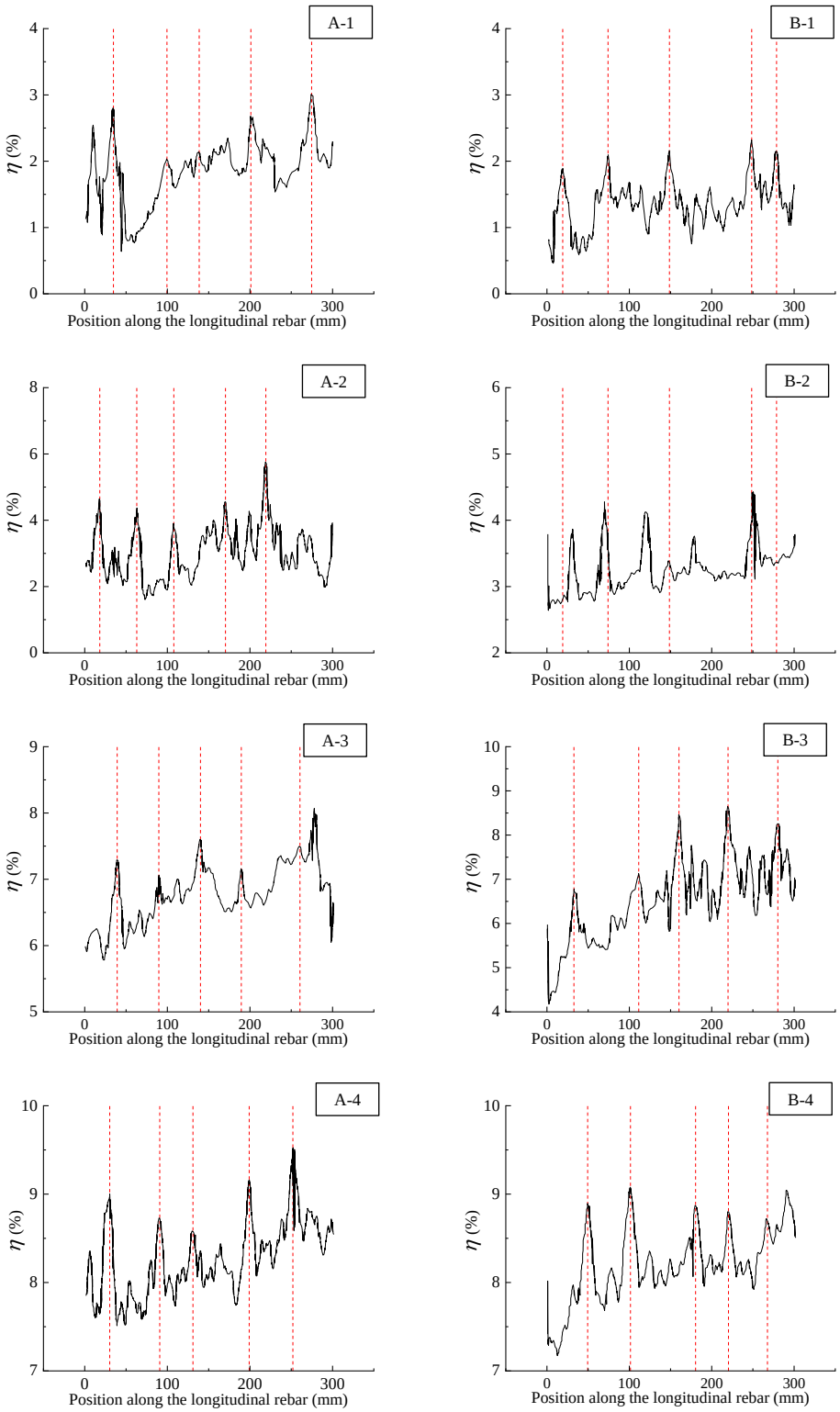


Figure 10. The value of η along the length of longitudinal rebars in tension zone (the red dashed lines indicate the positions of transverse cracks).

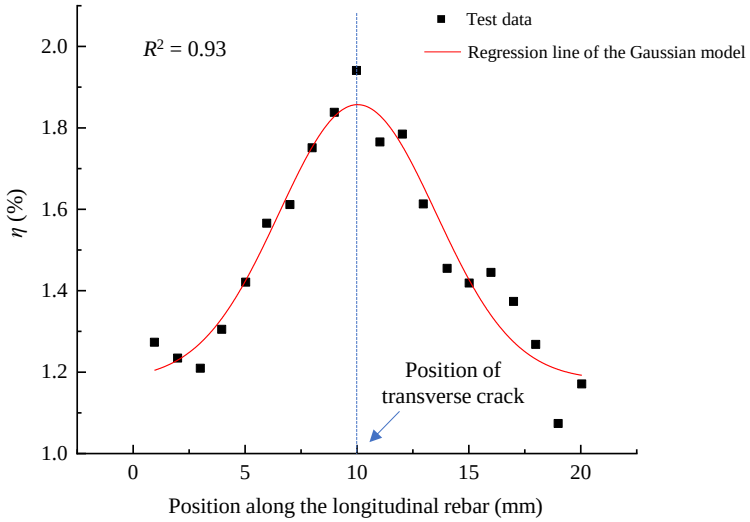
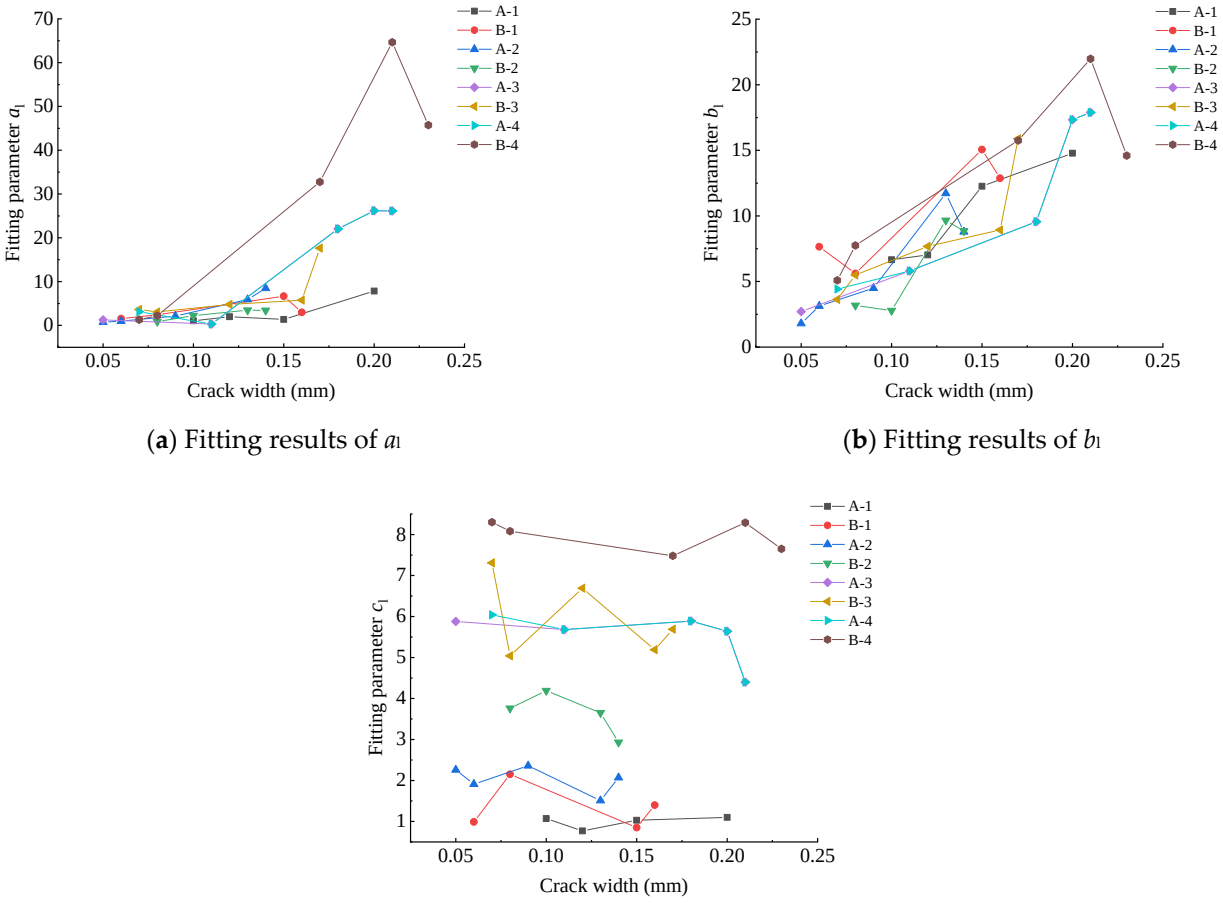


Figure 11. Fitting results of the distribution of corrosion rate in the cases of rebar A-2 with 0.14-mm crack width.

Table 2. Fitting results for corrosion rate distribution at transverse cracks.

Notation of Longitudinal Rebar	U.S. Size of Rebar (#)	Crack Width (mm)	z	a_1	b_1	c_1	R^2
A-1	#4	0.12	35	1.99	7.03	0.77	0.94
		0.15	101	1.36	12.26	1.03	0.84
		0.20	140	7.85	14.78	1.10	0.89
		0.15	205	2.19	6.82	0.85	0.80
		0.10	260	1.06	6.66	1.07	0.92
B-1	#4	0.06	23	1.54	7.65	0.99	0.84
		0.15	71	6.68	15.06	0.85	0.78
		0.16	150	2.99	12.87	1.40	0.96
		0.15	202	7.64	15.48	1.32	0.88
		0.08	265	2.43	5.61	2.15	0.91
A-2	#4	0.14	20	8.49	8.79	2.07	0.93
		0.13	59	5.92	11.72	1.51	0.87
		0.09	113	2.13	4.49	2.36	0.84
		0.05	168	0.74	1.8	2.26	0.90
		0.06	225	0.99	3.13	1.91	0.88
B-2	#4	0.08	33	2.13	4.03	2.85	0.92
		0.14	72	3.43	8.85	2.93	0.91
		0.13	124	3.48	9.66	3.65	0.88
		0.08	183	0.86	3.18	3.76	0.85
		0.10	249	2.24	2.78	4.19	0.67
A-3	#4	0.21	44	26.14	17.89	4.40	0.91
		0.11	93	0.31	5.8	5.68	0.76
		0.18	143	22.05	9.56	5.89	0.89
		0.20	191	26.19	17.34	5.64	0.88
		0.05	260	1.26	2.71	5.88	0.81
B-3	#4	0.16	35	5.76	8.93	5.19	0.91
		0.08	112	3.06	5.5	5.04	0.84
		0.12	165	4.79	7.68	6.69	0.83
		0.17	223	17.66	15.88	5.69	0.84
		0.07	277	3.63	3.63	7.31	0.57
A-4	#4	0.21	44	26.14	17.89	4.40	0.91
		0.11	93	0.31	5.8	5.68	0.76
		0.18	143	22.05	9.56	5.89	0.89
		0.20	191	26.19	17.34	5.64	0.88
		0.07	246	3.14	4.42	6.04	0.75
B-4	#4	0.23	51	45.74	14.6	7.65	0.95
		0.17	105	32.76	15.75	7.48	0.97
		0.21	180	64.66	21.98	8.29	0.63
		0.08	208	2.21	7.75	8.08	0.84
		0.07	263	1.31	5.09	8.30	0.93



(**a**) Fitting results of a_1

(**b**) Fitting results of b_1

(**c**) Fitting results of c_1

Figure 12. Results of fitting parameters in the cases of various crack widths.

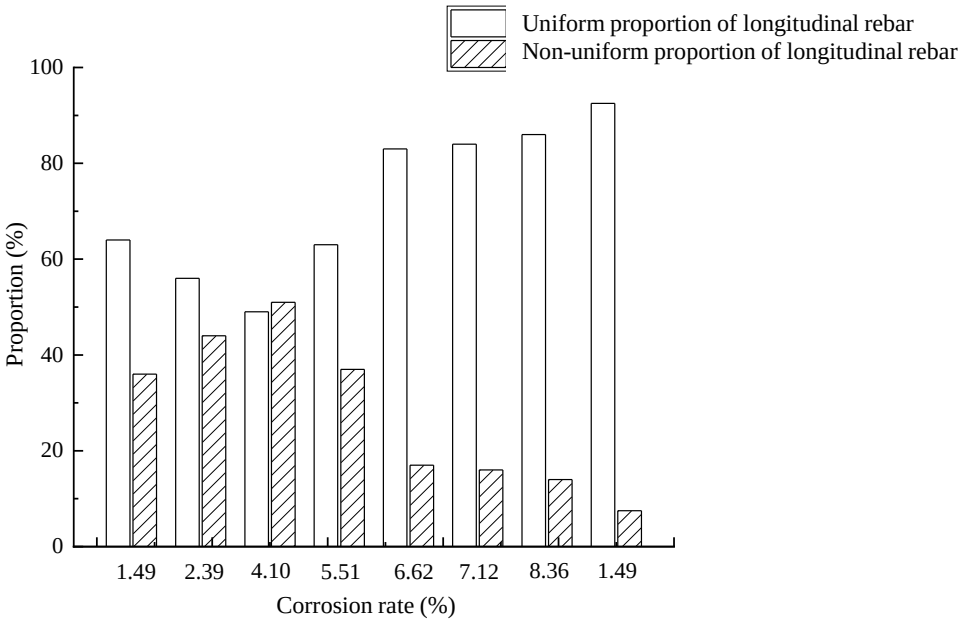


Figure 13. Percentages of uniform and non-uniform proportion with respect to corrosion of longitudinal rebar.

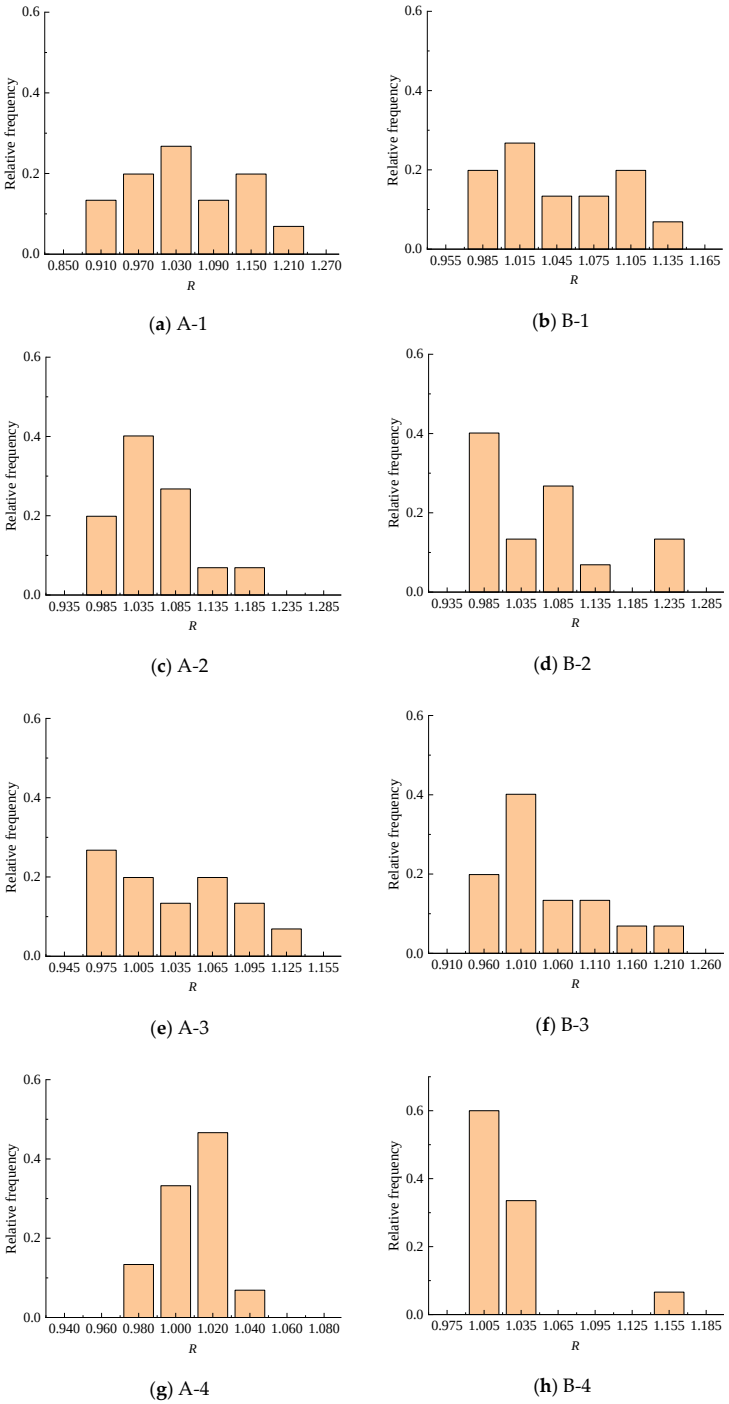
3.3. Effects of Stress Condition on the Longitudinal Non-Uniformity of Steel Corrosion

3.3.1. Non-Uniform Parameter Analysis of Corroded Steel Bars in Non-Stressed Section

The cross-sectional area spatial heterogeneity factor (R) is utilized to quantify the longitudinal non-uniformity of a corroded steel bar, as expressed in Equation (6). The corroded steel bar is divided by an interval of 20 mm. The frequency distribution histogram of R is obtained, as shown in Figure 14.

$$R = A_{av} / A_{min}, \tag{6}$$

where A_{av} is the average cross-sectional area of the corroded steel bar in the non-stressed section, A_{min} is the minimum cross-sectional area.



(**a**) A-1 (**b**) B-1

(**c**) A-2 (**d**) B-2

(**e**) A-3 (**f**) B-3

(**g**) A-4 (**h**) B-4

Figure 14. Frequency distribution of R-value for non-stressed sections.

In each 20 mm section, the R-values are arranged in the order of the largest to the smallest value (R_1, R_2, …, R_n). The total number of R-values is N. For the i_{th} value R_i, the empirical probability F_i can be calculated through Equation (7). As shown in Figure 15, each R-value has a good linear relationship with its corresponding $-\ln(\ln(1/F_i))$. The index R is validated to follow the Gumbel distribution. The K-S test was employed to test the fitness of the Gumbel distribution. According to the results of the test, the R-value conforms to the Gumbel distribution where the confidence level is 95%. The probability density function of the Gumbel distribution is shown in Equation (8). The mean value $E(R)$ and variance $D(R)$ of each group were statistically analyzed, as shown in Equations (9) and (10).

$$F_i = i/(N+1), \tag{7}$$

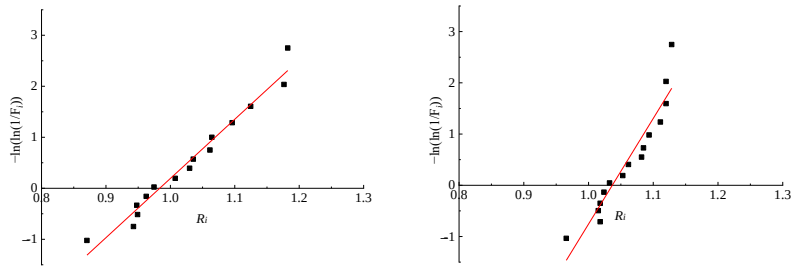
$$f(x) = \frac{1}{\sigma}\exp(-\frac{x-\mu}{\sigma})\exp\left[-\exp\left(-\frac{x-\mu}{\sigma}\right)\right], \tag{8}$$

where μ is the position parameter of the Gumbel distribution, and σ is the scale parameter of the Gumbel distribution.

$$E(R) = \mu + \lambda\sigma, \tag{9}$$

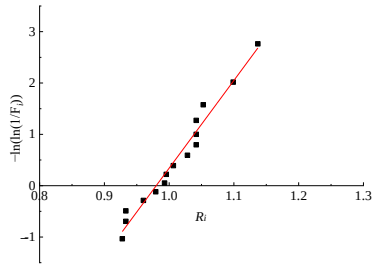
$$D(R) = \frac{\pi^2}{6}\sigma^2 \tag{10}$$

where λ is Euler's constant (λ = 0.5772).

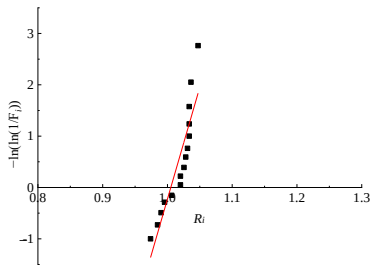


(**a**) A-1

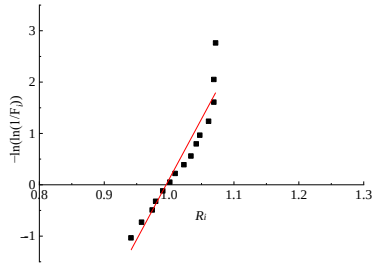
(**b**) B-1



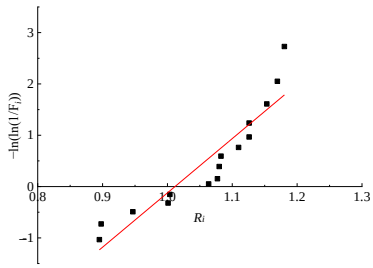
(**c**) A-2



(**d**) B-2

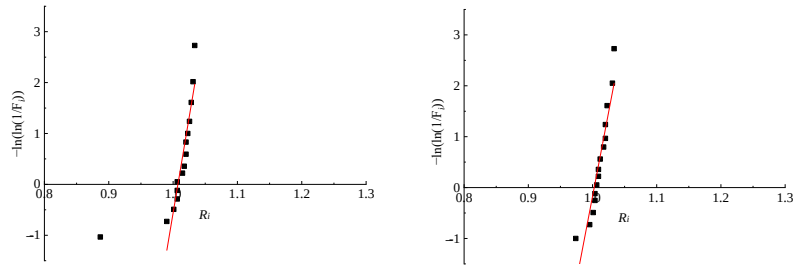


(**e**) A-3



(**f**) B-3

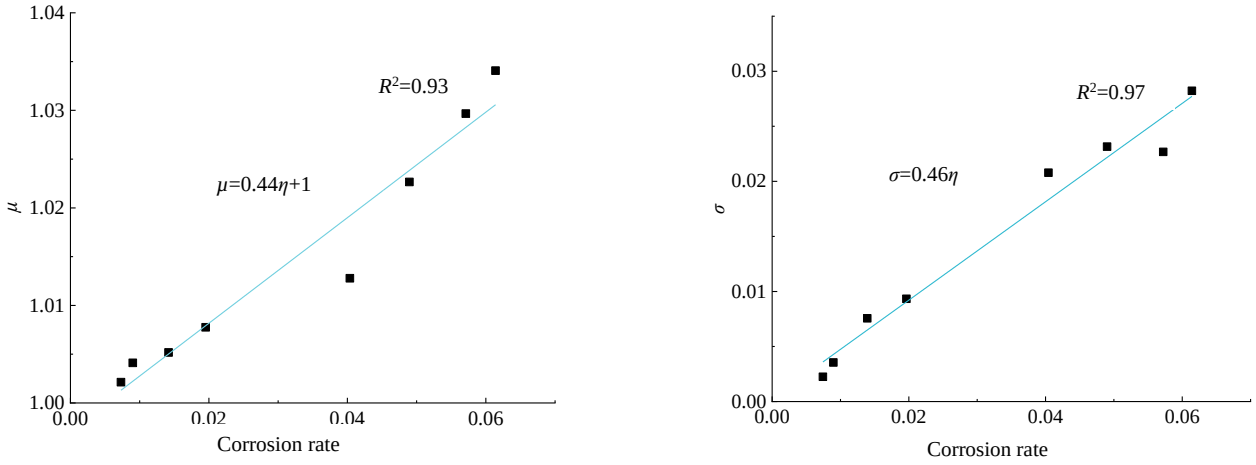
Figure 15. *Cont.*



(**g**) A-4 (**h**) B-4

Figure 15. Plots of *R*-value versus -ln(ln(1/F_i)) for the non-stressed section.

Figure 16 depicts the values of position parameters and scale parameters in the cases of different corrosion rates. As the corrosion rate increases, the position parameter and scale parameter increase linearly.



(**a**) (**b**)

Figure 16. Relationship between corrosion rate and (**a**) μ and (**b**) σ in non-stressed sections.

3.3.2. Non-Uniform Parameter Analysis of Corroded Steel Bars in Pure Bending Section

The linear relationship between non-uniform parameters and corrosion rate is consistent with the results obtained by other researchers [7,26]. Nevertheless, few studies investigate the distribution of the cross-sectional area spatial heterogeneity factor (*R*) in the cases of load-induced transverse cracks. In this regard, the non-uniform parameter analysis was carried out in the pure bending section. The corroded steel bar was divided into sections with an interval of 20 mm. Figure 17 shows the histogram of the *R*-value frequency distribution of the corroded steel bars in the pure bending section.

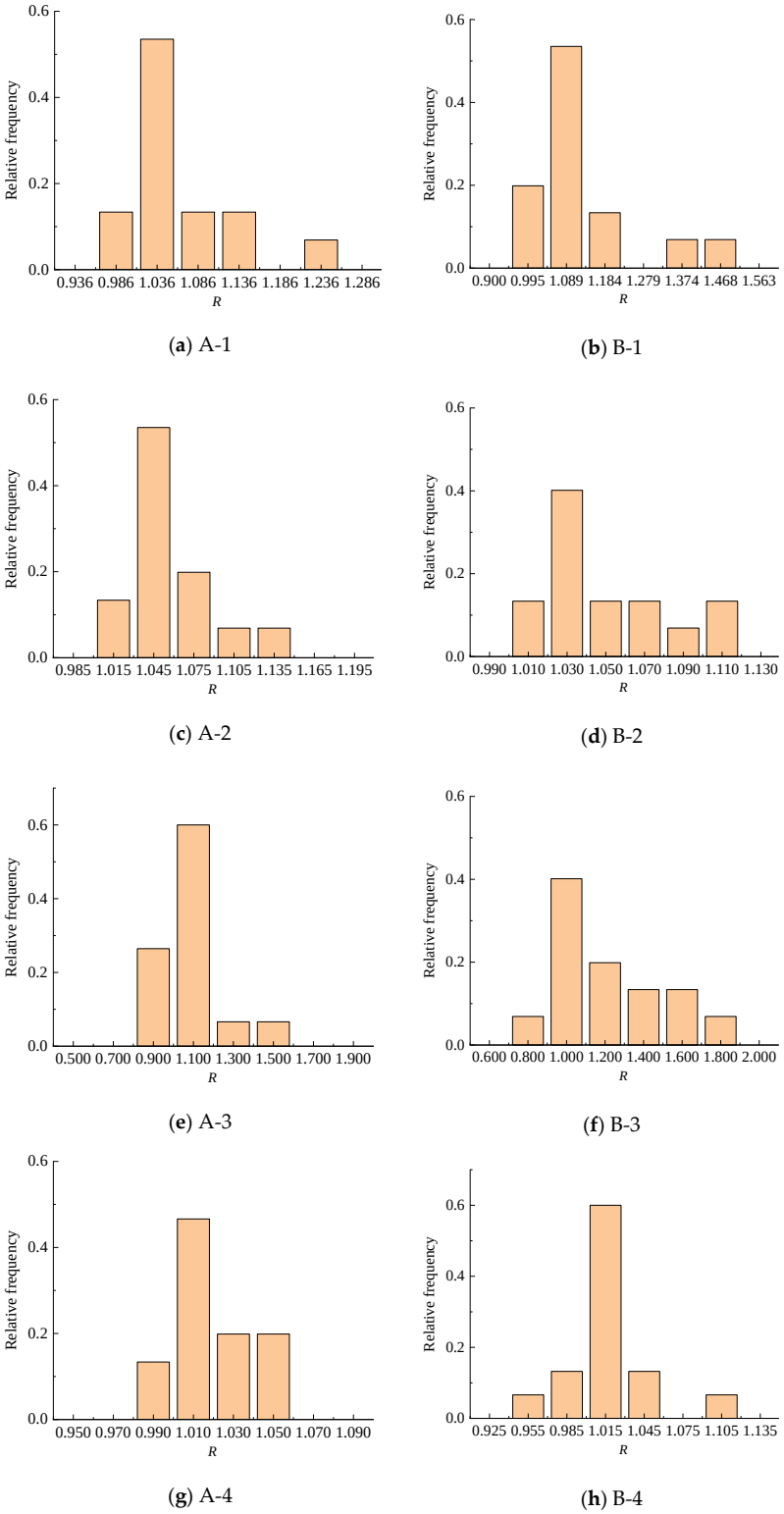
Similarly, based on Equation (7), each *R*-value has a good linear relationship with its corresponding $-\ln(\ln(1/F_i))$, as shown in Figure 18. The index *R* in the cases of the pure bending sections is validated to follow the Gumbel distribution.

With respect to the pure bending section, the values of parameters μ and σ in the cases of different corrosion rates are listed in Table 3. As can be seen, the obtained relationship between the corrosion rate of the non-stressed section and the parameters (μ and σ) shown in Figure 16 is not applicable to the stressed section. This may be due to the fact that the load-induced transverse cracks significantly influence the non-uniformity of corrosion for longitudinal steel, as presented in Figure 10. To describe the relationship between corrosion rate and non-uniform parameters (μ and σ) with the consideration of transverse cracks, two crack coefficients (α and β) are introduced, as shown in Equations (11) and (12). The crack coefficients (α and β) are correlated with load-induced transverse cracks. As can be

seen in Figure 19, linear relationships are demonstrated between the crack coefficients and the average value of transverse crack width ($\bar{w}_{av}$).

$$\mu = (\alpha + 0.44)\eta + 1, \tag{11}$$

$$\sigma = (0.46/\beta)\cdot\eta, \tag{12}$$



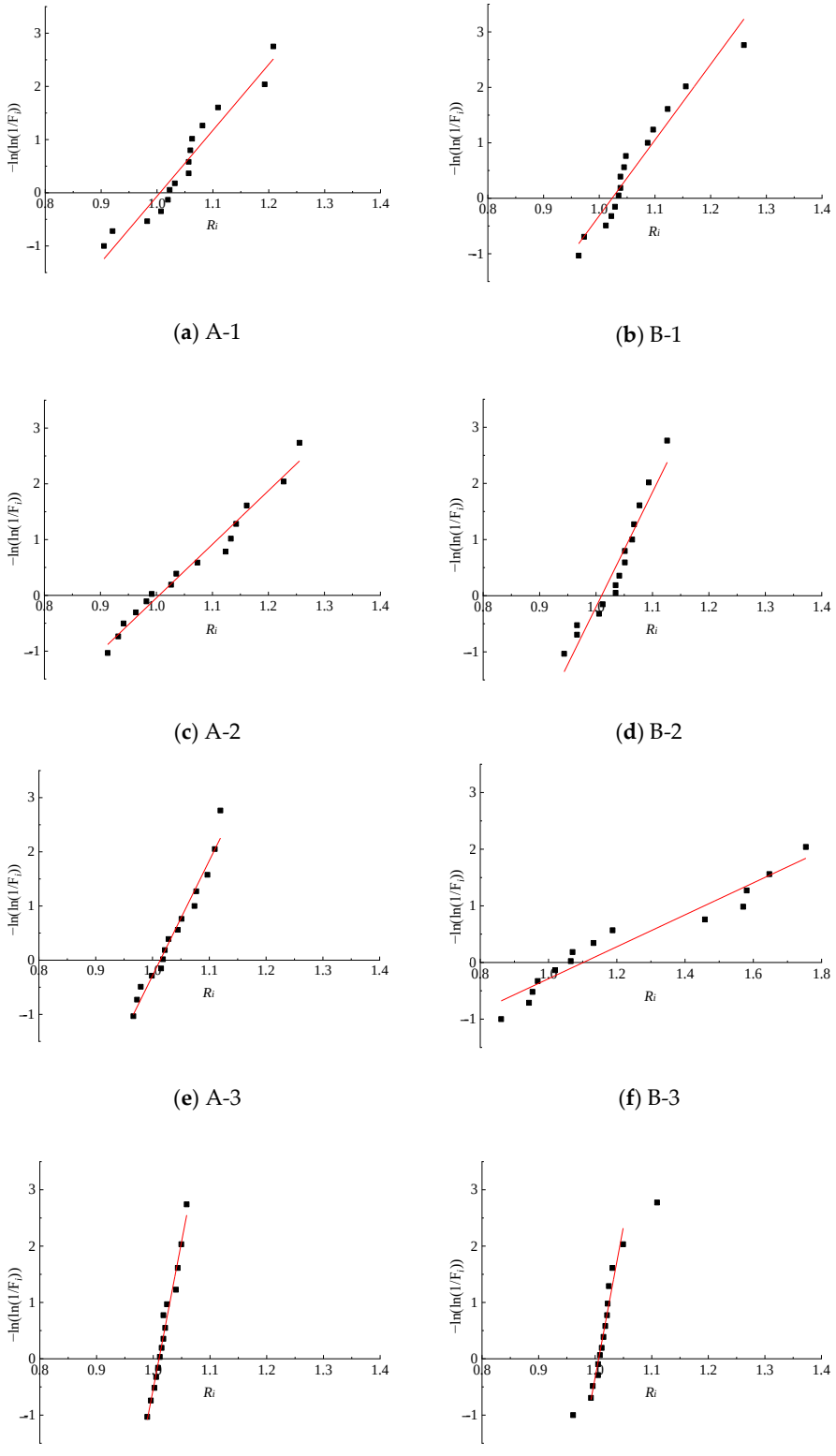
(**a**) A-1 (**b**) B-1

(**c**) A-2 (**d**) B-2

(**e**) A-3 (**f**) B-3

(**g**) A-4 (**h**) B-4

Figure 17. Frequency distribution of *R*-values for pure bending section.



(**a**) A-1 (**b**) B-1

(**c**) A-2 (**d**) B-2

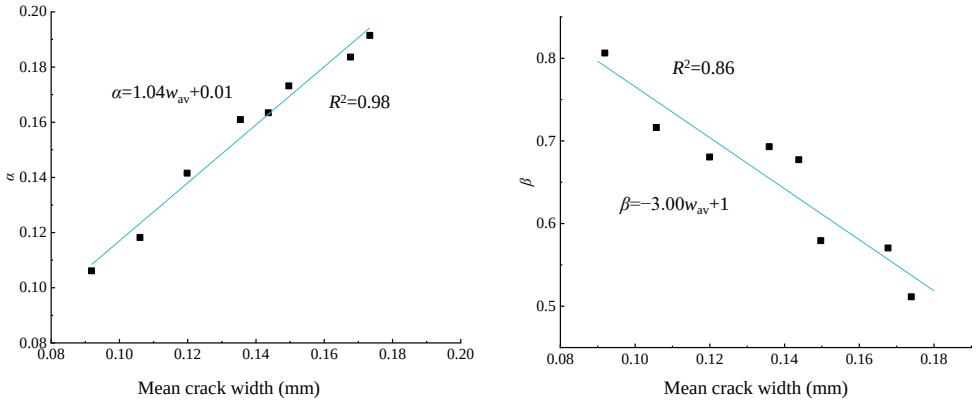
(**e**) A-3 (**f**) B-3

(**g**) A-4 (**h**) B-4

Figure 18. Plots of R-value versus $-\ln(\ln(1/F_i))$ for pure bending section.

Table 3. Results of parameters (μ and σ) in the case of pure bending section.

Corrosion Rate (%)	Position Parameter μ	Scale Parameter σ
1.49	1.0086	0.0101
2.39	1.0138	0.0162
4.10	1.0224	0.0234
5.51	1.0307	0.0354
6.62	1.0398	0.0535
7.12	1.0412	0.0474
8.36	1.0512	0.0664
8.61	1.0536	0.0774



(**a**) (**b**)

Figure 19. Relationship between mean crack width (w_{av}) and (**a**) α and (**b**) β in pure bending sections.

On the basis of Equations (11) and (12), in terms of the pure bending section, the non-uniform parameter μ can be described through Equation (13), while the non-uniform parameter σ is expressed in Equation (14). The position parameter μ is in a positive relationship with the corrosion rate and the mean crack width. In addition, the increasing rate of μ with the increase in the corrosion rate is proportional to the mean crack width. Under the same corrosion rate, a larger mean crack width leads to an increase in μ. The scale parameter σ also increases with the increase in the corrosion rate and a larger value of mean crack width results in a higher increasing rate of σ. Notedly, in the case of no crack width (i.e., $w_{av} = 0$), the results of the parameters obtained through Equations (13) and (14) are approximately equal to the results of the non-stressed section (Figure 16).

$$\mu = (1.04w_{av} + 0.01 + 0.44)\eta + 1, \quad (13)$$

$$\sigma = [0.46/(-3.00w_{av} + 1)] \cdot \eta, \quad (14)$$

The distribution of circumferential non-uniformity indicates the thickness of the rust layer. Considering the relationship between the expansive ratio of corrosion products and the thickness of the rust layer, corrosion-induced concrete cracking can be calculated [27–30]. On the other hand, the longitudinal non-uniformity of steel corrosion is significant in determining the position of steel occupying the smallest cross-sectional area, thereby calculating the load-bearing capacity of RC beams or columns subjected to mechanical load [5,6,9,31]. The present study considers the effect of sustained mechanical load on the non-uniformity of corrosion, which could be more similar to RC structures in engineering, compared to those without the consideration of mechanical load.

4. Conclusions

The present study investigated the circumferential and longitudinal non-uniformity of steel corrosion in concrete subjected to mechanical load. The following conclusions can be drawn:

(1) In the cases of concrete subjected to mechanical load, the distribution of rust layer thickness around the perimeter of the steel bar fits well with a Gaussian distribution. As the corrosion rate gradually increases, the non-uniform coefficient (a) is directly proportional to the maximum thickness of the rust layer, while the uniform coefficient (c) is linearly proportional to the minimum thickness of the rust layer.

(2) With respect to the longitudinal non-uniformity of reinforcement corrosion. It is observed that load-induced transverse cracks have a significant impact on the longitudinal distribution of reinforcement corrosion, leading to rust peaks near the locations of transverse cracks. In the vicinity of each rust peak, the corrosion rate of the steel bar follows a Gaussian distribution. In addition, the corrosion of steel bars tends to be more uniform with an increasing corrosion rate, and the longitudinal non-uniformity of steel bars is significant when the corrosion rate is low.

(3) In the case of non-stressed conditions, the cross-sectional area spatial heterogeneity factor (R) follows a Gumbel distribution. The position parameters (μ) and scale parameters (σ) are linearly related to the average corrosion rate of the reinforcement.

(4) In the case of the pure bending condition, the value of R follows a Gumbel distribution. Nevertheless, the relationship between corrosion rate and the non-uniform parameters (μ and σ) can hardly be applicable. This is mainly due to the development of transverse cracks in the pure bending sections under the influence of mechanical loads. Two crack influence coefficients (α and β) are introduced to describe the impact of mean transverse crack width on the frequency distribution parameters of R-values.

Author Contributions: Conceptualization, Z.D. and C.F.; methodology, K.X. and C.F; formal analysis, M.Y., W.N. and B.W.; writing—original draft preparation, Z.D. and B.W.; writing—review and editing, J.S. and W.N.; funding acquisition, B.W., C.F. and J.S. All authors have read and agreed to the published version of the manuscript.

Funding: This research was funded by the Center for Balance Architecture, Zhejiang University, grant number 281410-I52100.

Data Availability Statement: Some or all data, models, or code that support the findings of this study are available from the corresponding author upon reasonable request.

Conflicts of Interest: The authors declare no conflicts of interest.

References

1. Dong, Z.; Fu, C.; Lu, C.; Nóvoa, X.R.; Ye, H. Effect of stress on the critical chloride content of steel bar in simulated concrete pore solution. *J. Mater. Civ. Eng.* **2023**, *35*, 04023350. [CrossRef]
2. Fu, C.; Huang, J.; Dong, Z.; Song, C.; Zhang, Y. Shear behavior of reinforced concrete beams subjected to accelerated non-uniform corrosion. *Eng. Struct.* **2023**, *286*, 116081. [CrossRef]
3. Zhao, Y.; Zhang, X.; Ding, H.; Jin, W. Non-uniform distribution of a corrosion layer at a steel/concrete interface described by a Gaussian model. *Corros. Sci.* **2016**, *112*, 1–12. [CrossRef]
4. Ahmad, S.; Al-Huri, M.A.; Al-Osta, M.A.; Maslehuddin, M.; Al-Gadhib, A.H. An experimental approach to evaluate the effect of reinforcement corrosion on flexural performance of RC beams. *Buildings* **2022**, *12*, 2222. [CrossRef]
5. Zhu, W.; François, R.; Zhang, C.; Zhang, D. Propagation of corrosion-induced cracks of the RC beam exposed to marine environment under sustained load for a period of 26 years. *Cem. Concr. Res.* **2018**, *103*, 66–76. [CrossRef]
6. Jiang, C.; Ding, H.; Gu, X.L.; Zhang, W.P. Failure mode-based calculation method for bending bearing capacities of normal cross-sections of corroded reinforced concrete beams. *Eng. Struct.* **2022**, *258*, 114113. [CrossRef]
7. Chen, S.; Duffield, C.; Miramini, S.; Nasim Khan Raja, B.; Zhang, L. Life-cycle modelling of concrete cracking and reinforcement corrosion in concrete bridges: A case study. *Eng. Struct.* **2021**, *237*, 112143. [CrossRef]
8. Bossio, A.; Imperatore, S.; Kioumarsi, M. Ultimate flexural capacity of reinforced concrete elements damaged by corrosion. *Buildings* **2019**, *9*, 160. [CrossRef]

9. Zhang, B.; Wang, J.; Wu, B.; Guo, X.W.; Wang, Y.J.; Chen, D.; Zhang, Y.C.; Du, K.; Oguzie, E.E.; Ma, X.L. Unmasking chloride attack on the passive film of metals. *Nature* **2018**, *9*, 2559. [CrossRef]
10. Zhang, W.P.; Zhou, B.B.; Gu, X.L.; Dai, H.C. Probability distribution model for cross-sectional area of corroded reinforcing steel bars. *J. Mater. Civ. Eng.* **2014**, *26*, 822–832. [CrossRef]
11. Wang, X.; Song, X.; Zhang, M.; Du, X. Experimental comparison of corrosion unevenness and expansive cracking between accelerated corrosion methods used in laboratory research. *Constr. Build. Mater.* **2017**, *153*, 36–43. [CrossRef]
12. Zeng, B.; Wang, Y.; Gong, F.; Maekawa, K. Corrosion-induced cracking pattern analysis of RC beam under sustained load considering the poromechanical characteristics of corrosion products. *Buildings* **2022**, *12*, 2256. [CrossRef]
13. Shi, J.; Ming, J. Accelerated corrosion behavior of steel in concrete subjected to sustained flexural loading using electrochemical methods and X-ray computed tomography. *J. Mater. Civ. Eng.* **2018**, *30*, 1–12. [CrossRef]
14. Zhu, W.; Dai, J.; Poon, C. Prediction of the bond strength between non-uniformly corroded steel reinforcement and deteriorated concrete. *Constr. Build. Mater.* **2018**, *187*, 1267–1276. [CrossRef]
15. Wang, X.; Zhang, W.; Gu, X.; Dai, H. Determination of residual cross-sectional areas of corroded bars in reinforced concrete structures using easy-to-measure variables. *Constr. Build. Mater.* **2013**, *38*, 846–853. [CrossRef]
16. Fu, C.; Jin, N.; Ye, H.; Liu, J.; Jin, X. Non-uniform corrosion of steel in mortar induced by impressed current method: An experimental and numerical investigation. *Constr. Build. Mater.* **2018**, *183*, 429–438. [CrossRef]
17. Zhao, Y.; Xu, X.; Wang, Y.; Dong, J. Characteristics of pitting corrosion in an existing reinforced concrete beam exposed to marine environment. *Constr. Build. Mater.* **2020**, *234*, 117392. [CrossRef]
18. *GB 50010-2010*; Code for Design of Concrete Structures. China Planning Press: Beijing, China, 2015. (In Chinese)
19. Zhang, W.; Chen, J.; Luo, X. Effects of impressed current density on corrosion induced cracking of concrete cover. *Constr. Build. Mater.* **2019**, *204*, 213–223. [CrossRef]
20. Dang, V.; François, R. Influence of long-term corrosion in chloride environment on mechanical behaviour of RC beam. *Eng. Struct.* **2013**, *48*, 558–568. [CrossRef]
21. Zhang, W.; François, R.; Wang, R.; Cai, Y.; Yu, L. Corrosion behavior of stirrups in corroded concrete beams exposed to chloride environment under sustained loading. *Constr. Build. Mater.* **2021**, *274*, 121987. [CrossRef]
22. *ASTM G1-03*; Standard Practice for Preparing, Cleaning, and Evaluating Corrosion Test. ASTM: West Conshohocken, PA, USA, 2003.
23. Hiemer, F.; Jakob, D.; Keßler, S.; Gehlen, C. Chloride induced reinforcement corrosion in cracked and coated concrete: From experimental studies to time-dependent numerical modeling. *Mater. Corros.* **2018**, *69*, 1526–1538. [CrossRef]
24. Dong, Z.; Gu, X.-L.; Jin, Z.-H.; Poursaee, A.; Ye, H. Experimental and numerical investigations on the rate-limiting step for macrocell corrosion of reinforcing steel in concrete. *J. Mater. Civ. Eng.* **2022**, *34*, 04021407. [CrossRef]
25. Wang, K. Study on the Non-Uniform Corrosion Distribution of Steel Bars and Corrosion-Induced Cracking of Reinforced Concrete Structures. Master's Thesis, Zhejiang University, Hangzhou, China, 2018.
26. Liu, X.; Zhang, W.; Gu, X.; Ye, Z. Probability distribution model of stress impact factor for corrosion pits of high-strength prestressing wires. *Eng. Struct.* **2021**, *230*, 111686. [CrossRef]
27. Chen, J.; Zhang, W.; Gu, X. Modeling time-dependent circumferential non-uniform corrosion of steel bars in concrete considering corrosion-induced cracking effects. *Eng. Struct.* **2019**, *201*, 109766. [CrossRef]
28. Fang, X.; Pan, Z.; Chen, A. Phase field modeling of concrete cracking for non-uniform corrosion of rebar. *Theor. Appl. Fract. Mech.* **2022**, *121*, 103517. [CrossRef]
29. Wang, L.; Liang, Y.; Ueda, T. Numerical simulation of corrosion-induced cracking of concrete considering rust penetration into cracks. *J. Mater. Civ. Eng.* **2021**, *33*, 04021183. [CrossRef]
30. Van Steen, C.; Van Beirendonck, T.; Vrijdaghs, R.; Hendriks, M.A.N.; Verstrynge, E. A two-phased modelling approach for corrosion-induced concrete cracking and bond deterioration in reinforced concrete. *Eng. Struct.* **2023**, *294*, 116624. [CrossRef]
31. He, Z.; He, C.; Ma, G.; Yang, W.; Kang, X. Performance assessment of partially corrosion-damaged RC segment incorporating the spatial variability of steel corrosion. *Constr. Build. Mater.* **2023**, *371*, 130789. [CrossRef]

Disclaimer/Publisher's Note: The statements, opinions and data contained in all publications are solely those of the individual author(s) and contributor(s) and not of MDPI and/or the editor(s). MDPI and/or the editor(s) disclaim responsibility for any injury to people or property resulting from any ideas, methods, instructions or products referred to in the content.